# Mesoporous silica materials from diluted and concentrated solutions of nonionic fluorinated and ionic hydrogenated surfactants mixtures

Karine Assaker, Marie-José Stébé, Jean-Luc Blin

# Mesoporous Silica Materials from Diluted and Concentrated solutions of Nonionic Fluorinated and Ionic Hydrogenated Surfactants Mixtures

Karine Assaker, Marie-José Stébé and Jean-Luc Blin*

Université de Lorraine/CNRS, SRSMC, UMR7565, F-54506 Vandoeuvre-lès-Nancy cedex, France

* Corresponding authors:

Pr. Jean-Luc Blin
Université de Lorraine
SRSMC UMR 7565
Faculté des Sciences et Technologies
BP 70239
F-54506 Vandoeuvre-lès-Nancy cedex, France
Tel. +33 3 83 68 43 70
E-mail: Jean-Luc.Blin@univ-lorraine.fr

**Keywords**: Mixed surfactant systems; Mixed micelles, Liquid Crystals, Mesoporous silica

**Abstract**

Herein, mesostructured silica materials have been prepared through both the cooperative self-assembly and liquid crystal templating mechanisms by using mixtures of polyoxyethylene fluoroalkylether and cationic quaternary ammonium surfactants as building blocks. The nonionic surfactant /ionic surfactant /water phase diagram shows that a micellar phase (L1) was formed. The SAXS spectra of the two surfactants micellar phases are different from that of micelles constituted of only one component. This provides informations about the nature of the micelles, which are really mixed. A detailed investigation of the liquid crystals domain was also conducted, and results indicate the presence of a hexagonal mixed phase.

Then, mesoporous silica materials with high specific surface area have been synthesized, using surfactant mixtures, and characterized by small angle X-ray scattering, transmission electron microscopy and nitrogen adsorption-desorption analysis. The SAXS patterns show two hexagonal porous networks, showing the presence of the dual porosity.

## 1. Introduction

Porous inorganic materials with tunable, hierarchical pore structures are becoming more and more important as a class of solid materials because of their wide variety of applications such as support for catalysts, or biomedical applications such as drug delivery [1-4]. Their importance comes from their properties such as a large surface area (around 1000 $m^2/g$ for silica), their large pore volume, and the presence of pores that allows the control of the diffusion [7-8]. The use of adapted templates for the preparation of these materials permits the tuning of the pore sizes as well as the other properties in order to meet the requirements of any application. One method to prepare these porous materials consists in using organized molecular systems. For example ordered mesoporous silica can be synthesized from micelles according to the cooperative templating mechanism (CTM) [9-14]. In that case following the interactions between the micelles and the hydrolyzed precursor, intermicellar polymerization occurs leading to the formation of a hybrid mesophase which gives the mesoporous material after surfactant removal. These mesostructured silica compounds can also be prepared by using the liquid crystal templating (LCT) mechanism, also called transcriptive mechanism, for which the inorganic precursors grow directly around the liquid crystal used as imprint. After the polymerization and the condensation, the template can be removed, leaving a mesoporous material whose structure, pore size and symmetry are determined by the liquid crystal scaffold [15-17]. Based on this concept, macroporous materials can be obtained from emulsions [18-21]. The transcriptive and the cooperative mechanisms can also be combined to get hierarchical porous materials, which exhibit porosity at different levels. These kinds of mesostructures have interest for applications, for example, in catalysis or adsorption. Indeed, it was reported that a hierarchical combination of pores reduces transport limitations in catalysis, resulting in higher activities and better controlled of selectivity [22]. The development of hierarchical porous materials has therefore attracted much interest over the

past few years and in the literature many papers are focused on the synthesis of meso-macro, micro-macro or micro-mesoporous materials [23-29]. For example, combining the CTM mechanism with the emulsions templating, one macro-mesoporous silica can be synthesized. In that case we start from oil-in-water emulsion where the oil droplets are dispersed in the continuous phase that is a direct microemulsion. The oil droplets are stabilized by the surfactant molecules. Upon the addition of the inorganic precursor, its polymerization occurs around the oil droplets but also around the swelled micelles by oil, which constitute the microemulsion. After hydrothermal treatment and the organic removal, the obtained material exhibits porosity at two levels : the macropores, which are the imprints of the emulsion oil droplets and the mesopores which are formed by the micelles according to the CTM mechanism [25]. Among the different surfactant-based systems used to prepare these porous materials, fluorinated ones are of peculiar interest [30-32]. Indeed, thanks to their high thermal stability, the hydrothermal treatment required for the inorganic polymerization can be performed at higher temperature. So its level of condensation is increased and as a consequence the obtained materials have a higher hydrothermal stability than the ones prepared with hydrogenated surfactants under the same conditions [33].

Due to their interesting properties that cannot be found in individual surfactant, importance of mixed systems has been increasingly recognized in the last few years [34-37]. In some cases even new properties are found since they provide synergistic behavior [34,36,37] and this make them very useful for applications such as emulsifying, dispersing, wetting, flotation, washing and cleaning ability [37]. In particular, mixtures of hydrogenated and fluorinated surfactants are useful in many practical applications [38-40]. Indeed, the presence of fluorine atom provides to these mixtures unique chemical and thermal properties, which allow their applications under severe conditions compared to the hydrocarbon amphiphiles. Due to the non-ideal net repulsive interactions occurring between the fluorocarbon and hydrocarbon

chains, which have different polarities, micellar solutions of hydrogenated and fluorinated surfactants mixtures are either composed of mixed micelles containing both surfactants in a well-defined proportion or of two kinds of micelles enriched in one of the two components [34,36,38,41-45]. Therefore these mixed systems are excellent candidates to design hierarchical porous silica and in particular dual mesoporous materials. In this study mixtures of a polyoxyethylene fluoroalkyl ether [$R^F_8(EO)_9$] and a cationic hydrogenated surfactant, cethyltrimethylammonium bromide (CTABr), have been used to prepare dual mesoporous silica either through the CTM or the LCT mechanisms. Prior the materials' synthesis, we have investigated in detail the $R^F_8(EO)_9$/CTABr/water system since the properties of the recovered silica are related to the ones of the surfactants based system used for their preparation.

## 2. Materials and methods

The used fluorinated surfactant, which was provided by DuPont, has an average chemical structure of $C_8F_{17}C_2H_4(OC_2H_4)_9OH$. It is labeled as $R^F_8(EO)_9$. The hydrophilic chain moiety exhibits a Gaussian chain length distribution and the hydrophobic part is composed of well defined mixture of fluorinated tails. The selected hydrogenated surfactant is the ionic cethyltrimethylammonium bromide noted CTABr of chemical formula ($C_{16}H_{33}N(CH_3)_3Br$), which was purchased from Aldrich.

***2.1. Phase diagram :*** The samples were prepared by weighing the required amounts of fluorinated surfactant, CTABr and water in well-closed glass vials to avoid evaporation. They were left at controlled temperature for some hours in order to reach equilibrium. Liquid crystal phase domain was identified by its texture observed with optical microscope equipped with cross polarizers. In order to find the characteristics of liquid crystals and the limits of this domain, additional SAXS experiments were also performed. Samples studied by SAXS will be designated according to the surfactant mixtures as Hx/F(100-x), with H and F symbolize

the hydrogenated and fluorinated surfactants, respectively and x is the volume or weight percentage of hydrogen compound, when analyzing either micellar solutions or liquid crystal phases respectively.

***2.2. Mesoporous material preparation*:** Using the cooperative templating mechanism, silica materials have been prepared from mixed micellar solutions containing 10 wt.% of different mixtures CTABr/$R^F_8(EO)_9$ in water. The micellar solution prepared in acidic aqueous solution of HCl of 1.2 M and brought to 40°C. Then, the precursor of silica, tetramethoxysilane (TMOS) was added. The amount of TMOS was determined from the molar ratio surfactant/TMOS noted R, which was fixed at 0.5. The mixture was homogenized and then transferred into a sealed Teflon autoclave to carry out hydrothermal treatment in an oven at 100 °C for 1 day. When the dual mesoporous materials were synthesized from LCT : 1 g of the surfactant mixture was first dissolved in tetramethoxysilane (TMOS), used as the silica source. The TMOS amount was calculated using the molar ratio (R) of mixed surfactant/TMOS equal to 0.175. The total surfactant concentrations corresponding to a direct hexagonal phase in the $R^F_8(EO)_9$/CTABr/water system was fixed to 62.5%. The CTABr/ $R^F_8(EO)_9$ weight ratio was varied from H0/F100 to H100/F0. Then in order to form the hexagonal liquid crystal phase, water was added. The pH of the solution was adjusted with hydrochloric acid (HCl) to 0.6. Afterwards, to remove the methanol produced during the hydrolysis of the silica precursor, the mixture was placed under vacuum. The obtained samples were heated at 70°C during 70 hours. Whatever the pathway, the final products were recovered after ethanol extraction with a Soxhlet apparatus during 24 hours.

***2.3 Characterization*** : Small Angle X-ray Scattering (SAXS) measurements were carried out on a SAXSess mc² instrument (Anton Paar), using a line collimation system. This instrument is attached to a ID 3003 laboratory X-Ray generator (General Electric) equipped with a sealed X-Ray tube (PANalytical, $\lambda_{Cu,\ K\alpha}$ = 0.1542 nm) operating at 40 kV and 50 mA. A multilayer

mirror and a block collimator provide a monochromatic primary beam. A translucent beam stop allows the measurement of an attenuated primary beam at q=0. Micelles were introduced into thin Special Glas capillaries (WJM Glas) with an outer diameter of 1.5 mm, before being placed inside an evacuated sample chamber at 20°C. The scattered intensities were registered by a CCD detector (Princeton Instruments, 2084 x 2084 pixels array with 24 x 24 µm² pixel size) at 309 mm distance from the sample. Using SAXSQuant software (Anton Paar), the 2D image was integrated into one-dimensional scattering intensities I(q) as a function of the magnitude of the scattering vector $q = (4\pi/\lambda) \sin(\theta)$, where $2\theta$ is the total scattering angle. All data were calibrated by normalizing the attenuated primary intensity and then were corrected for the background scattering from the empty capillary and the solvent, and for slit-smearing effects by a desmearing procedure from SAXSQuant software using the Lake method. After correction, intensities were scaled into absolute units using water as a reference material. Liquid crystals were put in a paste cell, before being placed inside an evacuated chamber equipped with a temperature controlled sample holder unit. Mesoporous materials were put between two sheets of Kapton® placed in a powder cell before being introduced inside the evacuated chamber. All data were corrected for the background scattering from the Kapton® and for slit-smearing effects by a desmearing procedure from SAXSQuant software using the Lake method. $N_2$ adsorption and desorption isotherms were determined on a Micromeritics TRISTAR 3000 sorptometer at –196 °C. The pore diameter and the pore size distribution were determined by the BJH (Barret, Joyner, Halenda) [46] method applied to the adsorption branch of the isotherm.

**Results and discussion**

## 3. Results and discussion

### 3.1. $R^F_8(EO)_9$/CTABr/water phase diagram

Because of the Kraft point of CTABr, the $R^F_8(EO)_9$/CTABr/water phase diagram has been established at 40°C (Fig. 1). In water pure $R^F_8(EO)_9$ forms a direct micellar phase ($L_1$) for concentrations lower than 40 wt.% [47], while $L_1$ is limited to concentrations of less than 25 wt.% in water for CTABr [48]. As shown in Figure 1, a micellar solution is obtained for total surfactant concentrations up to 40 wt.% if the percentage of $R^F_8(EO)_9$ in the mixture is higher than 20%. For lower fluorinated content, the $L_1$ domain exists between 40 and 25 wt.% of surfactant, depending on the $R^F_8(EO)_9$ quantity in the mixture. A Liquid crystal domain, for which only a hexagonal-type structure ($H_1$) is evidenced, appears from 50 to 28 wt.% of total surfactants in water. This region ($H_1$) joins the hexagonal phases of the two surfactant/water binary systems, which are present between 50 and 80 wt.% for the $R^F_8(EO)_9$ [47] and between 25 and 80 wt.% for the CTABr [48]. Despite the antagonistic properties of fluorinated and hydrogenated compounds, we observe the formation of large micellar and hexagonal mixed areas. To go further in the micelles' characterization, SAXS experiments have been performed. Figure 2A presents, the spectra on log-log scales and in absolute intensity of mixed micellar solutions with a total surfactant concentration of 5 wt.% in water for various ratios between the hydrogenated and the fluorinated compounds. CTABr micelles spectrum shows the presence of two large reflections. The first situated at 0.6 $nm^{-1}$ is a correlation peak and is due to the structure factor (interparticles interaction). The second peak situated at 1.2 $nm^{-1}$ characterizes the condensation of the counterions ($Br^-$) around the micelles forming a shell [49,50]. According to Aswal [49,50], micelles of CTABr are small and slightly elongated and their main dimensions are 4 and 2.4 nm. The spectrum of $R^F_8(EO)_9$ micelles does not show any correlation peak, but the scattering intensity is much higher than that of

CTABr, due to the presence of the fluorine atoms which has a much higher electron density than that of hydrogen. Previous studies by SAXS and SANS show that the pure fluorinated micelles are spheroidal objects slightly elongated and their main dimensions are 9 and 6.6 nm [51]. Looking at the spectra of the micellar phase obtained from the surfactants mixture, the scattered intensity increases with the increase of the proportion of the fluorinated surfactant. The correlation peak of CTABr micelles, at 0.6 $nm^{-1}$, is shifted to smaller q values (0.48 $nm^{-1}$) when the volume composition of the studied solutions passes from H66/F33 to H40/F60 (Fig. 2A). This feature suggests that, either mixed micelles or two types of micelles with different structure than the pure ones, are formed. Indeed, considering calculations of linear combinations of the pure fluorinated and the pure hydrogenated micelles, the correlation peak is not displaced and remains at 0.6 $nm^{-1}$, when the $R^F_8(EO)_9$ content in the surfactants mixture is increased (Figure 2B).

SAXS measurements were also applied on the $H_1$ domain in the $R_F^8(EO)_9$/CTABr/water system and the SAXS spectra of the mixed systems exhibit a typical profile three peaks with the relative peak positions, 1, $\sqrt{3}$, 2., defining the apparent existence of a single hexagonal lattice. Assuming that the mixture of surfactants formed a mixed entity, we have determined the structural parameters of the hexagonal liquid crystal phase. For a given composition the molar weight (M) of the mixed entity is:

$$M = \frac{n^F M^F + n^H M^H}{n^F + n^H}$$

where $n^F$ and $n^H$ respectively stands for the mole number of fluorinated and hydrogenated surfactant; $M^F$ and $M^H$ are the corresponding molar weight. The hexagonal phase is composed of infinite cylinders packed in a hexagonal array. In case of direct systems, cylinders are filled by the hydrophobic chains and are covered by both head groups and water. As depicted in

scheme 1, the distance $d_{10}$ associated to the first peak of the hexagonal structure is related to the hydrophobic radius $R_H$ by the relation [52]:

$$\frac{V_B}{V_{TA} + \alpha V_E} = \frac{\sqrt{3}\pi R_H^2}{2d_{10}^2}$$

where α stands for the number of water molecules per surfactant molecule and $V_B$, $V_{TA}$, $V_E$ respectively stand for the molar volumes of the hydrophobic part of the mixed surfactant, the mixed surfactant and water ($V_E$ = 18 cm³/mol). $V_B$ and $V_{TA}$ depend on the molar ratio between the two amphiphiles. For example, for a mixture composed of 30 wt.% of CTABr and 70 wt.% of $R^F_8(EO)_9$, these values are $V_B$ = 276.7 and $V_{TA}$ = 519.4 $cm^3$/mol. The values of $V_{TA}$ and $V_B$ for the pure surfactant were calculated from densities and are $V_{TA}$ = 626, $V_B$ = 261 $cm^3$/mol for $R^F_8(EO)_9$ and $V_{TA}$ = 404 and $V_B$ = 293 $cm^3$/mol for CTABr. The cross-sectional area S (Scheme 1) can then be deduced from the following relation [52]:

$$S = \frac{2V_B}{N R_H}$$

N is the Avogadro number.

Figure 3A depicts the evolution of the repetition spacing $d_{10}$ as a function of the number of water molecules per surfactant molecule (α). A decrease of $d_{10}$ is observed for the mixed hexagonal phase compared to the pure fluorinated hexagonal one, regardless the water fraction in the mixture. We also note that for the three mixtures considered, H70/F30, H60/F40 and H30/F70, $d_{10}$ increases linearly with α. The increase of $d_{10}$ with the water content is due to the hydration of the head group and the formation of a water film surrounding the surfactant cylinders. Beyond a value of α equal to 36, 38 and 43 for mixture surfactants of H70/F30, H60/F40, H30/F70, respectively, water is no longer incorporated in the hexagonal phase and the system becomes biphasic. As shown in Figure 3B, the hydrophobic radius ($R_H$) doesn't vary significantly with the amount of water (α); it slightly increases when the mixed entity is enriched in CTABr. Values of the hydrophobic radius pass from 1.6 to 1.8 ± 0.04 nm by considering two extremes mixtures H30/F70 and H70/F30.

Taking into account the values of the different bonds, we can estimate that the length of the extended chains of $R^F_8(EO)_9$ (8 fluorinated and 2 hydrogenated carbon atoms) and (CTABr) ($C_{16}$) are respectively 1.4 and 2.2 nm. Comparing these values to the hydrophobic radius, we can conclude that the hydrophobic chains of CTABr are semi-folded, while those of $R^F_8(EO)_9$ are probably extended.

The polar head surface remains constant, regardless proportions of both surfactants in the mixture, and is equal to 0.55 ± 0.02 $nm^2$ (Fig. 3B). This value is larger than that of pure CTABr (0.49 $nm^2$) and that of $R^F_8(EO)_9$ (0.50 $nm^2$), likely due to the folding of the hydrophobic chains of CTABr.

### 3.2. Mesoporous silica

After the investigation of the $R^F_8(EO)_9$/CTABr/water system, porous materials have been prepared according to both the cooperative and the transcriptive mechanisms. When micelles are used as building blocks, the mesoporous materials synthesized from both the pure fluorinated surfactant or the pure CTABr micellar solutions exhibit a hexagonal mesopore ordering, characterized by the presence of the (100), (110) and (200) reflections at 5.2, 3.0 and 2.6 nm for $R^F_8(EO)_9$ and at 4.0, 2.3 and 2.0 nm for CTABr (Fig. 4A). Adding up to 30% of CTABr in the surfactant mixture, no significant change is noted in the SAXS patterns. This suggests that only one kind of micelles is formed and that the micellar solution is composed of $R^F_8(EO)_9$ micelles which have incorporated the CTABr molecules. Reaching 30% of CTABr in the mixture, a shoulder on the (10) reflection line is observed. Its intensity increases as a function of the CTABr content. By comparison with the pattern of the material prepared with the pure CTABr, this supplementary reflection can be attributed to a network templated by hydrogenated-rich micelles. So, as reflecting by the SAXS analysis of the micellar solution, two kinds of micelles, having different structure than the pure ones, are

present in the solution. The TEM images (Fig. 5) of silica materials prepared in this range of surfactant concentrations clearly show a regular mesopore ordering, but it is not possible to distinguish the presence of two porous networks. Beyond 70%, a further increase of the CTABr content leads to a single network, meaning that only one type of mixed micelles is formed again and that CTABr micelles have accommodated the fluorinated molecules.

Whatever the proportion between the two surfactants, a type IV isotherm is obtained by nitrogen adorption-desorpotion analysis (Fig. 6A), meaning that the materials are mesoporous [53]. The isotherm of the material prepared with $R^F_8(EO)_9$ shows an inflectio due to capillary condensation starting at a relative pressure of 0.45. When the CTABr is added the inflection moves toward smaller values of relative pressure. Since the $p/p_0$ position of the inflection point is related to the pore diameter, it can be inferred that a decrease of the mean pore diameter occurs when the loading of CTABr is raised. Beyond 50% of hydrogenated surfactant in the mixture, the isotherms are similar to that of silica prepared using pure CTABr. However, it should be noted that even if the coexistence of two mesopores networks is detected by SAXS, only one inflection point, related to the capillary condensation step, is detected on the isotherm. It can be deduced that the two mesopores sizes are close to each other. This is further confirmed by the mesopores size distribution, for which only maximum is noted. However this is not surprising since materials templated by pure fluorinated and hydrogenated surfactants have very close values of mesopores diameter, 3.8 and 3.2, respectively (inset of Fig.6A). Hence when prepared from the surfactant mixture, it is not possible to clearly distinct the two mesopores networks detected by SAXS. It should also be noted that at very low relative pressure the shape of the isotherms suggests also the presence of micropores. The specific surface area of materials prepared with the mixed system CTABr/$R^F_8(EO)_9$ increases from ~ 900 to 1250 $m^2/g$ when the weight fraction of CTABr increases from 0 to 100 (Fig. 7A). The reverse trend is noted for the pore diameter, which

decreases with the increase of wt.% of CTABr (Fig. 7B), while the pore volume remains approximately constant around 1 $cm^3/g$ (Table 1). The morphology of the mesoporous silica particles was observed by scanning electron microscopy (SEM) (Fig. 8). SEM images show spheroidal or cord shaped particles, regardless the composition of micelles. By contrast, we notice that the particles size slightly decreases when the surfactant mixture becomes richer in $R^F_8(EO)_9$.

Preparing the silica materials thought the transcriptive mechanism, all materials exhibit a hexagonal mesopore ordering, characterized by the presence of the (100), (110) and (200) reflections. Materials prepared with pure $R^F_8(EO)_9$ exhibit SAXS pattern with reflections at 5.0, 2.8 and 2.5 nm, and those prepared with pure CTABr give SAXS pattern with reflections situated at 3.6, 2.0 and 1.8 nm (Fig. 4B). When the CTABr wt.% increases in the surfactants mixture the intensity of the first reflection on the SAXS patterns decreases gradually. These results are similar to that obtained when materials are prepared using the CTM (Fig. 4A). For materials prepared with CTABr content between 40 and 70%, in addition to three reflections of a hexagonal lattice an additional reflection is observed at 4.7 nm (Fig. 4B). This indicates the coexistence of two channels arrays. However, it should be reminded that in contrary to the micellar phase, the investigation of the hexagonal liquid crystal domain has shown that the latter is composed only of a single hexagonal lattice. Therefore it could be assumed that in the presence of TMOS, the limits of the different domains of the phase diagram will be shifted and that the phenomenon of demixing will take place, leading to a biphasic system containing a fluorinated-rich $H_1^F$ phase in equilibrium with a hydrogenated-rich hexagonal phase $H_1^H$. However, as observed for the materials prepared through the CTM, isotherms obtained by adsorption-desorption of nitrogen show that the silica materials prepared with a CTABr content lower than 70 present only one inflection point due to capillary condensation ( Fig. 6B) and a single pore diameter is evidenced regardless the weight proportion of

CTABr/$R^F_8(EO)_9$ (inset of Fig. 6B). Once again at very low relative pressure the shape of the isotherm is characteristic of the presence of micropores. When the mixture of surfactants is composed predominantly of CTABr (> 70%), the materials exhibit an isotherm that can be qualified as intermediate between type I and IV is observed. According to Dubinin [54], this kind of isotherm is characteristic of super-microporous materials, *i.e.* the pore size is located at the limit between the micro and mesoporous domain. This feature was confirmed by the pore size distribution type. Whatever the CTABr content, the specific surface area is high (> 1100 $m^2/g$), the pore volume remains around 0.75 $cm^3/g$ and a gradual decrease in pore diameter, which does not exceed 0.8 nm, is noted from Table 1.

**Conclusion**

Mesoporous materials have been prepared using mixtures of ionic hydrogenated and nonionic fluorinated surfactants according to both the cooperative and the transcriptive mechanisms. The phase behavior of the CTABr-$R^F_8(EO)_9$ mixture in aqueous solution was first established at 40°C. SAXS experiments shows that the micellar solution is composed of either only one type of mixed micelles or of two types of micelles having a different structure than the pure fluorinated and the pure hydrogenated micelles. The hexagonal liquid crystal domain is composed only of a mixed structure. We have also determined the structural parameters of this $H_1$ phase. No variation of the cross sectional area and of the hydrophobic radius with the number of water molecules per surfactant molecule is noted.

Whatever the synthesis pathway, the SAXS spectra reveals the coexistence of two mesopores networks but only one size can be detected by nitrogen adsorption-desorption analysis. This indicates that the values of the two mesopores sizes are too closed to each other to be distinguished. In any case the shape of the isotherm at very low relative pressure show that micropores are present in the mesoporous silica materials.

**ACKNOWLEDGEMENTS:**

Authors would like to thank DuPont de Nemours Belgium for providing the fluorinated surfactant

**References**

[1] L. F. F. P. G. Braganca, M. Ojeda, J.L.G. Fierro, M.I. Pais da Silva, Bimetallic Co-Fe nanocrystals deposited on SBA-15 and HMS mesoporous silicas as catalysts for Fischer-Tropsch synthesis, Appl. Catal. A-Gen. 423-424 (2012) 146-153.

[2] P. Botella, A. Corma, M. Quesada, Synthesis of ordered mesoporous silica templated with biocompatible surfactants and applications in controlled release of drugs, J. Mater. Chem. 22 (2012) 6394-6401.

[3] P. Perego, R. Millini, Porous materials in catalysis: challenges for mesoporous materials, Chem. Soc. Rev. 42 (2013) 3956-3976.

[4] S.Y. Park, M. Barton, P. Pendleton, Mesoporous silica as a natural antimicrobial carrier, Colloids and Surfaces A: Physicochem. Eng. Aspects 385 (2011) 256-261.

[5] C.S. Cundy, P.A. Cox, The hydrothermal synthesis of zeolites: history and development from the earliest days to the present time, Chem. Rev. 103 (2003) 663-702.

[6] H.P. Hentze, M. Antonietti, Template synthesis of porous organic polymers, Curr. Opin. Solid. St. M 5 (2001) 343-353.

[7] F. Schüth, Endo- and exotemplating to create high-surface-area inorganic materials, Angew. Chem. Int. Ed. 42 (2003) 3604-3622.

[8] B.T. Holland, C.F. Blanford, T. Do, A. Stein, Synthesis of highly ordered, three-dimensional, macroporous structures of amorphous or crystalline inorganic oxides, phosphates, and hybrid composites, Chem. Mater. 11 (1999) 795-805.

[9] C. T. Kresge, W. J. Roth, The discovery of mesoporous molecular sieves from the twenty year perspective, Chem. Soc. Rev. 42 (2013) 3663-3670.

[10] C.T. Kresge, M.E. Leonowicz, W.J. Roth, J.C. Vartuli, J.S. Beck, Ordered mesoporous molecular sieves synthesized by a liquid-crystal template mechanism, Nature 359 (1992) 710-712.

[11] D. Zhao, Q. Huo, J. Feng, B.F. Chmelka, G.D. Stucky, Nonionic triblock and star diblock copolymer and oligomeric surfactant syntheses of highly ordered, hydrothermally stable mesoporous silica structures, J. Am. Chem. Soc. 120 (1998) 6024-6036.

[12] S.A. Bagshaw, E. Prouzet, T.J. Pinnavaia, Templating of mesoporous molecular sieves by nonionic polyethylene oxide surfactants, Science 269 (1995) 1242-1244.

[13] Y. Wan, D. Zhao, On the controllable soft-templating approach to mesoporous silicates, Chem. Rev. 107 (2007) 2821-2860.

[14] J. L. Blin, M. Impéror-Clerc, Mechanism of self-assembly in the synthesis of silica mesoporous materials: in situ studies by X-ray and neutron scattering, Chem. Soc. Rev. 42 (2013) 4071-4082.

[15] G. S. Attard, J.C. Glyde, C.G. Göltner, Liquid-crystalline phases as templates for the synthesis of mesoporous silica, Nature 378 (1995) 366-368.

[16] S.A. El-Safty, Y. Kiyozumi, T. Hanaoka, F. Mizukami, Controlled design of ordered and disordered pore architectures, geometries, and dimensions of HOM-type mesostructured monoliths and their hydrothermal stabilities, J. Phys. Chem. C 112 (2008) 5476-5489.

[17] K. Zimny, J.L. Blin, M.J. Stébé, Ordered mesoporous silica Templated by nonionic fluorinated liquid crystals, J. Phys. Chem. C 113 (2009) 11285-11293.

[18] A. Imhof, D.J. Pine, Uniform macroporous ceramics and plasrics by emulsions templating, Adv. Mater. 10 (1998) 697-700.

[19] H. Zhang, G.C. Hardy, M.J. Rosseinsky, A.I. Copper, Uniform emulsion-templated silica beads with high pore volume and hierarchical porosity, Adv. Mater. 15 (2003) 78-81.

[20] B.P. Binks, Macroporous silica from solids-stabilized emulsion templates, Adv. Mater. 14 (2002) 1824-1827.

[21] C. Oh, S.C. Chung, S.I. Shin, Y.C. Kim, S.S. Im, S.G. Oh, Distribution of macropores in silica particles prepared by using multiple emulsions, J. Colloids Interface Sci 254 (2002) 79-86.

[22] M.O. Coppens, G.F. Froment, The effectiveness of mass fractal catalysts, Fractals 5 (1997) 493-505.

[23] T. Sen, GJT. Tiddy, J.L. Casci, M.W Anderson, macro-cellular silica foams: synthesis during the natural creaming process of an Oil-in-Water Emulsion, Chem. Commun. 17 (2003) 2182-2183.

[24] K. Nakanishi, Y. Kobayashi, T Amatani, K. Hirato, T. Kodaira, Spontaneous formation of hierarchical macro-mesoporous ethane-silica monolith Chem. Mater. 16 (2004) 3652-3658.

[25] J.L. Blin, B. Bleta, J. Ghanbaja, M.J. Stébé, Fluorinated emulsions: Templates for the direct preparation of macroporous–mesoporous silica with a highly ordered array of large mesopores Microporous and Mesoporous Mater. 94 (2006) 74-80.

[26] H. Mori, M. Uota, D. Fujikawa, T. Yoshimura, T. Kuwahara, G. Sakai, T. Kijima, Synthesis of micro-mesoporous bimodal silica nanoparticles using lyotropic mixed surfactant liquid-crystal templates, Microporous and Mesoporous Mater. 91 (2006) 172-180.

[27] O. Sel, D. Kuang, M. Thommes, B. Smarsly, Principles of hierarchical meso-macropore architectures by liquid crystallline and polymer colloid templating Langmuir 22 (2006) 2311-2322.

[28] J. Nestor, A. Víchez, C. Solans, J. Esquena, Facile Synthesis of meso/macroporous dual materials with ordered mesopores using highly concentrated emulsions based on a cubic liquid crystal, Langmuir 29 (2013) 432-440.

[29] J Esquena, J. Nestor, A. Vílchez, K. Aramaki, C. Solans, Preparation of mesoporous/macroporous materials in highly concentrated emulsions based on cubic phases by a single-step method, Langmuir 2012 (28) 12334-12340.

[30] J.L. Blin, M.J. Stébé, Effect of fluorocarbon addition on the structure and pore diameter of mesoporous materials prepared with a fluorinated surfactant, Microporous and Mesoporous Mater. 87 (2005) 67-76.

[31] J. Esquena, C. Rodriguez, C. Solans, H. Kunieda, Formation of mesostructured silica in nonionic fluorinated surfactant systems Microporous and Mesoporous Mater. 92 (2006) 212-219.

[32] B. Tan, A. Dozier, H.J. Lehmler, B. Knutson, S.E. Rankin, Elongated silica nanoparticles with a mesh phase mesopore structure by fluorosurfactant templating Langmuir 20 (2004) 6981-6984.

[33] F. Michaux, C. Carteret, M.J. Stébé, J.L. Blin, Hydrothermal stability of mesostructured silica prepared using a nonionic fluorinated surfactant, Microporous and Mesoporous Mater. 116 (2008) 308-317.

[34] B. Kronberg, Surfactant mixtures, Curr. Opin. Colloid Interface Sci. 2 (1997) 456-463.

[35] M. Almgren, Mixed micelles and other structures in the solubilization of bilayer lipid membranes by surfactants., Biochim. Biophys. Acta. 1508 (2000) 146-63.

[36] F. Petit, I. Iliopoulos, R. Audebert, S. Szönyi, Associating Polyelectrolytes with

Perfluoroalkyl Side Chains: Aggregation in Aqueous Solution, Association with Surfactants, and Comparison with Hydrogenated Analogues, Langmuir. 13 (1997) 4229-4233.

[37] F. Jost, H. Leiter, M.J. Schwuger, Synergisms in binary surfactant mixtures, Colloid Polym. Sci. 266 (1988) 554-561.

[38] V. Peyre, Segregation phenomena in micelles from mixtures of fluorinated and hydrogenated surfactants, Curr. Opin. Colloid Interface Sci. 14 (2009) 305-314.

[39] E. Blanco, C. Rodriguez-Abreu, P. Schulz, J.M. Ruso, Effect of alkyl chain asymmetry on catanionic mixtures of hydrogenated and fluorinated surfactants, J. Colloid Interface Sci. 341 (2010) 261-266.

[40] M. Almgren, V.M. Garamus, L. Nordstierna, J.L. Blin, M.J. Stébé, Nonideal mixed micelles of fluorinated and hydrogenous surfactants in aqueous solution. NMR and SANS studies of anionic and nonionic systems, Langmuir. 26 (2010) 5355-5363.

[41] K. Ogiono, M. Abe (eds), *Mixed Surfactant Systems*, Surfactant Science Series, (1993), Vol. 46, Dekker Inc. : New York.

[42] Kissa (ed), *Fluorinated Surfactants Synthesis properties Applications*; Surfactant Science Series, (1994), Vol. 50; Dekker : New York.

[43] K. Shinoda, T. Nomura, Miscibility of fluorocarbon and hydrocarbon surfactants in micelles and liquid mixtures. Basic studies of oil repellent and fire extinguishing agents, J. Phys. Chem. 84 (1980) 365-369.

[44] P. Barthélémy, V. Tomao, J. Selb, Y. Chaudier, B. Pucci, Fluorocarbon−Hydrocarbon nonionic surfactants mixtures: A study of their miscibility, Langmuir 18 (2002) 2557-2563.

[45] M. Almgren, V.M. Garamus, Small Angle Neutron Scattering study of demixing in micellar solutions containing CTAC and a partially fluorinated cationic surfactant J. Phys. Chem. B, 109 (2005) 11348-11353.

[46] E.P. Barrett, L.G. Joyner, P.P. Halenda, The Determination of Pore Volume and Area Distributions in Porous Substances. I. Computations from Nitrogen Isotherms, J. Am. Chem. Soc. 73 (1951) 373-380.

[47] J.L. Blin, P. Lesieur, M.J. Stébé, Nonionic Fluorinated Surfactant: Investigation of Phase Diagram and Preparation of Ordered Mesoporous Materials, Langmuir. 20 (2004) 491-498.

[48] K. Shigeta, M. Suzuki, H. Kunieda, Phase behavior of polyoxyethylene oleyl ether in water, Prog. Colloid Polym. Sci. 106 (1997) 49-51.

[49] V.K. Aswal, Small-Angle Scattering from Micellar Solutions, Bhabha At. Res. Cent. Newsl. (2001) 37-42.

[50] V.K. Aswal, P.S. Goyal, H. Amenitsch, S. Bernstorff, Counterion condensation in ionic micelles as studied by a combined use of SANS and SAXS, Pramana- J. Phys. 63 (2004) 333-338.

[51] F. Michaux, J.-L. Blin, J. Teixeira, M.J. Stébé, Structural investigation of nonionic fluorinated micelles by SANS in relation to mesoporous silica materials., J. Phys. Chem. B. 116 (2012) 261–8.

[52] M. Alibrahim, M.J. Stébé, G. Dupont, J.C. Ravey, Effect of an Ionic Surfactant on the Phase Behavior of a Nonionic Surfactant-Based System, J. Chim. Phys. Phys.-Chim. Biol. 94 (1997) 1614-1633

[53] K. S. W. Sing, D. H. Everett, R. A. W. Haul, L. Moscou, R. A. Pierotti, J. Rouquerol, T. Siemieniewska, Reporting physisorption data for gas/solid systems with special

reference to the determination of surface area and porosity (Recommendations 1984) IUPAC, Pure and Appl. Chem. 57 (1985) 603-619.

[54] M.M. Dubinin in : Progress in Surface and Membrane Science, 9 (D.A. Cadenhead, Ed.) Academic Press, New York, (1975), p. 1.

**Figures captions**

Scheme 1 : Scheme showing the relation between the distance ($d_{10}$) associated to the first peak of the hexagonal structure, the hydrophobic radius ($R_H$) and the cross-sectional area (S).

Figure 1: Partial composition (wt.%) phase diagram of the $R^F_8(EO)_9$/CTABr/water system at 40°C.

Figure 2 : SAXS patterns of micellar solutions CTABr/$R^F_8(EO)_9$, with a total surfactant concentration in water of 5 wt.% (A) and linear combinations of pure fluorinated and pure hydrogenated micelles (B).

Figure 3 : Hexagonal liquid crystals: Evolution of d-spacing (A), of the hydrophobic radius, $R_H$, and the cross-sectional area, S, (B) as a function of α, the number of water molecules per surfactant molecule.

Figure 4 : Mesoporous materials : Evolution of the SAXS pattern as a function of the CTABr content (wt.%) in the surfactant mixture. Materials are prepared either through the CTM (A) or the LCT (B) pathway.

Figure 5 : Mesoporous materials : TEM images as a function of the CTABr content (wt.%) in the surfactant mixture. Materials are prepared through the CTM mechanism.

Figure 6 : Mesoporous materials : Nitrogen adsorption-desorption isotherms with the corresponding pore size distribution (inset) as a function of the CTABr content (wt.%) in the surfactant mixture. Materials are prepared either through the CTM (A) or the LCT (B) pathway.

Figure 7 : Mesoporous materials Variation of the specific surface area (A) and of the pore diameter (B) with the content of CTABr (wt.%) in the surfactant mixture.

Figure 8 : Mesoporous materials : SEM images of silica mesoporous materials prepared by CTM with two different CTABr weight percent in the surfactant mixture.

Table 1 : Specific surface area ($S_{BET}$), pore diameter (Ø) and total pore volume ($V_P$) of silica materials prepared by CTM and LCT mechanism using different CTABr/$R^F_8(EO)_9$ (H/F) proportions.

| | Cooperative Templating Mechanism (CTM) | | | Liquid Crystal Templating (LCT) | | |
|---|---|---|---|---|---|---|
| H/F | $S_{BET}$ ($m^2.g^{-1}$) | Ø(nm) | Vp ($cm^3/g$) | $S_{BET}$ ($m^2.g^{-1}$) | Ø (nm) | Vp ($cm^3/g$) |
| H0/F100 | 829 | 3.8 | 1.1 | 1192 | 3.0 | 0.85 |
| H10/F90 | 925 | 3.6 | 1.1 | 1170 | 2.5 | 0.71 |
| H15/F85 | 902 | 3.5 | 1.1 | | | |
| H20/F80 | 997 | 3.3 | 1.1 | 1230 | 2.9 | 0.78 |
| H25/F75 | 971 | 3.3 | 1.1 | | | |
| H40/F60 | 1010 | 2.9 | 1.1 | 1182 | 2.5 | 0.78 |
| H50/F50 | 1072 | 2.8 | 1.1 | 1220 | 2.3 | 0.75 |
| H60/F40 | 1062 | 2.9 | 1.2 | 1167 | 2.3 | 0.70 |
| H70/F30 | 1053 | 2.8 | 1.1 | 1367 | 2.0 | 0.57 |
| H80/F20 | 1172 | 2.9 | 1.3 | 1297 | 2.2 | 0.68 |
| H90/F10 | 1275 | 2.8 | 1.2 | 1400 | 2.0 | 0.51 |
| H100/F0 | 1134 | 3.2 | 1.3 | 1545 | -- | -- |

**Scheme 1 :**

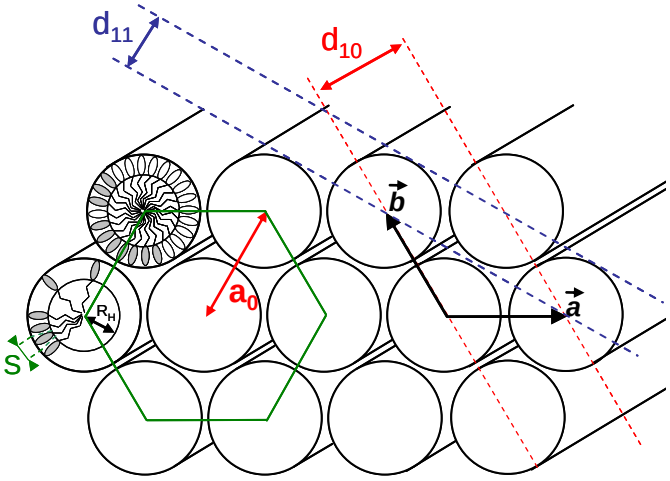

**Figure 1**

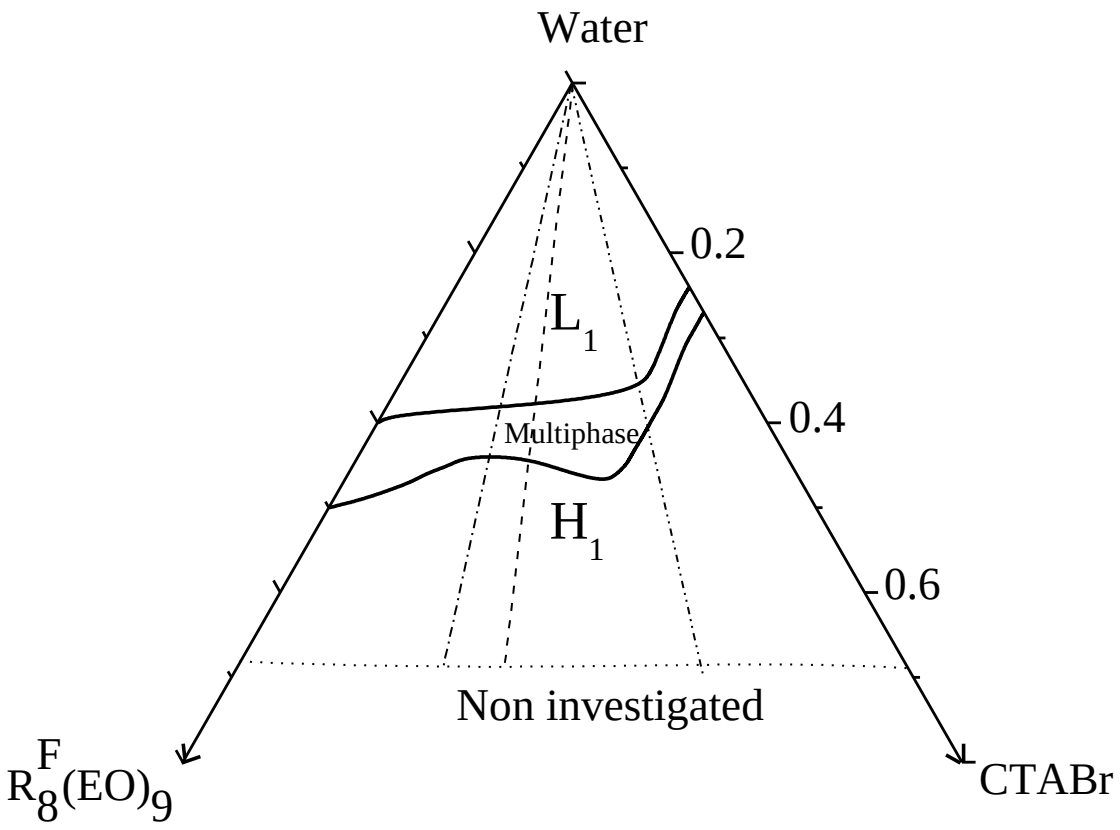
Water
0.2
0.4
0.6
$L_1$
Multiphase
$H_1$
Non investigated
$R_8^F(EO)_9$
CTABr

**Figure 2**

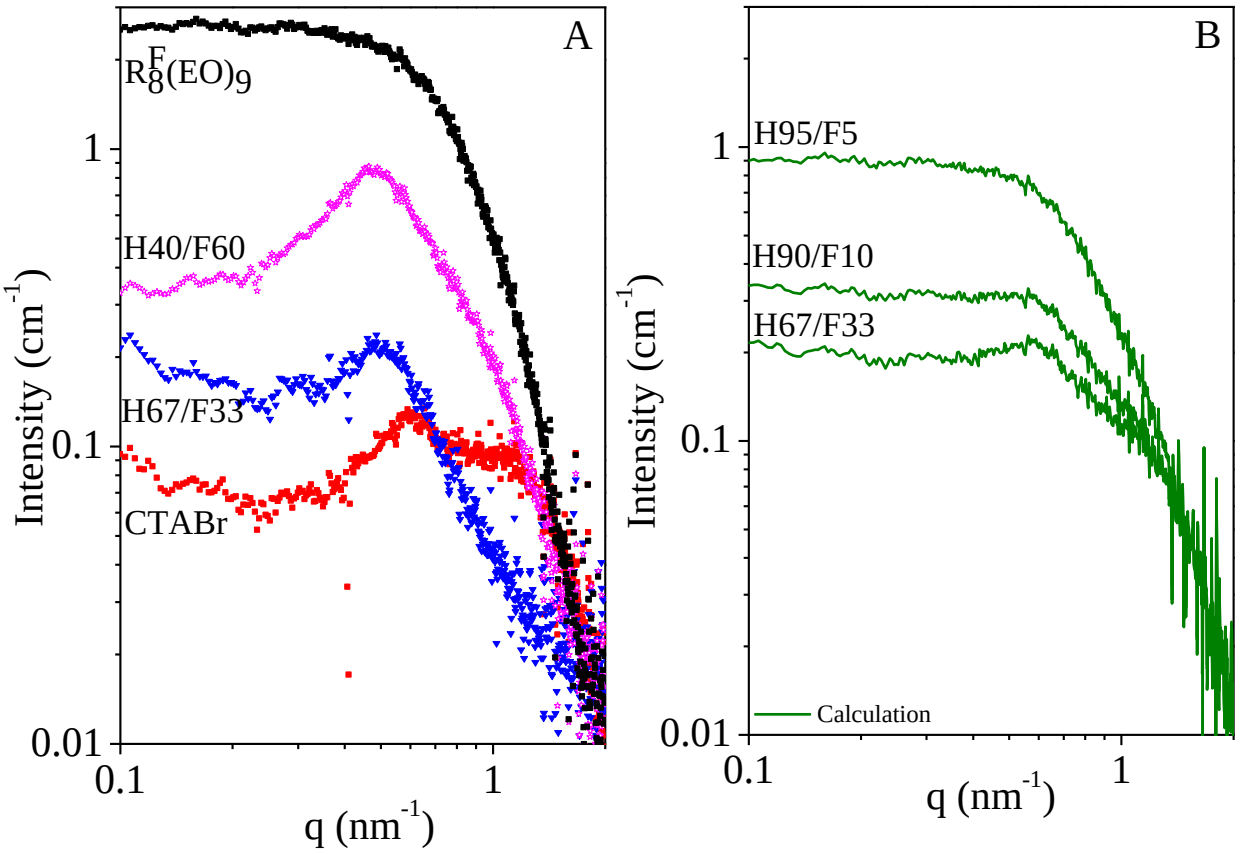
A
$R_8^F(EO)_9$
H40/F60
H67/F33
CTABr
Intensity (cm$^{-1}$)
q (nm$^{-1}$)
1
0.1
0.01
0.1
1
B
H95/F5
H90/F10
H67/F33
Calculation
Intensity (cm$^{-1}$)
q (nm$^{-1}$)
1
0.1
0.01
0.1
1

**Figure 3**

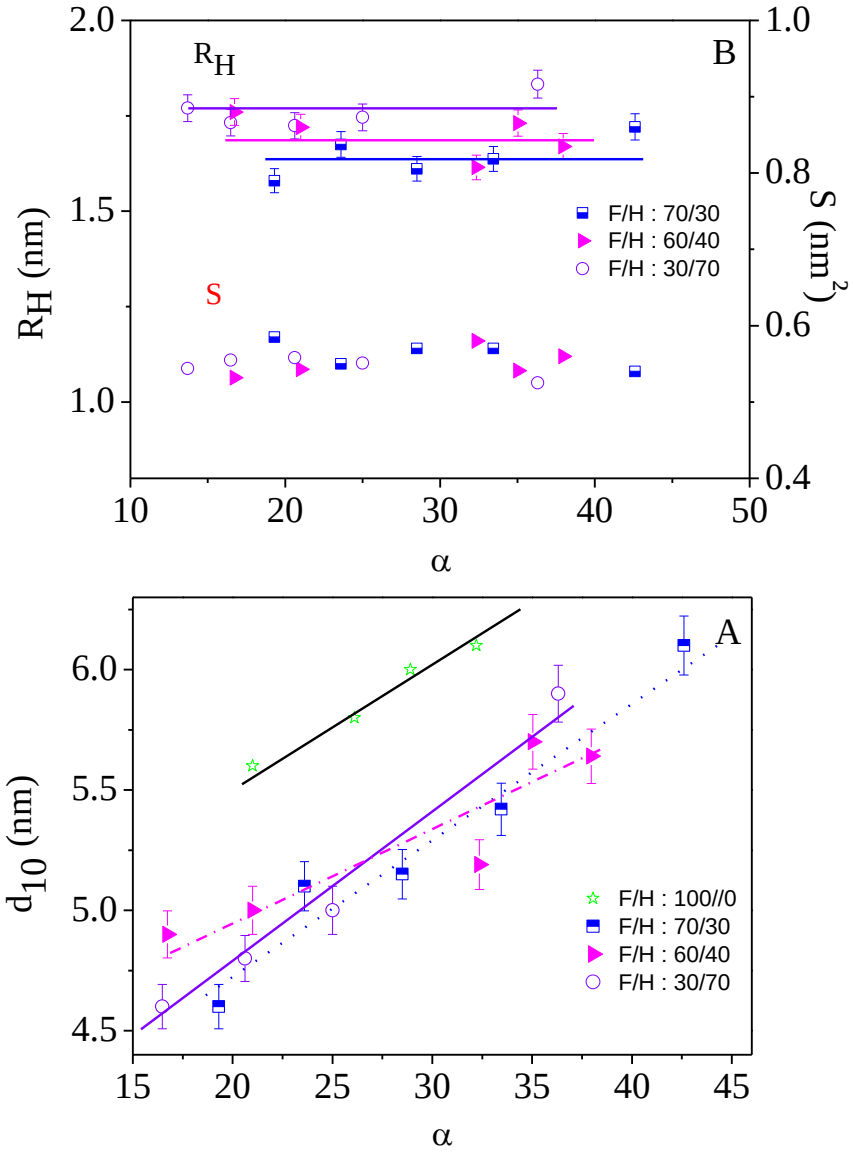
B
$R_H$
S
F/H : 70/30
F/H : 60/40
F/H : 30/70
$R_H$ (nm)
S ($nm^2$)
α
A
$d_{10}$ (nm)
F/H : 100//0
F/H : 70/30
F/H : 60/40
F/H : 30/70
α

**Figure 4**

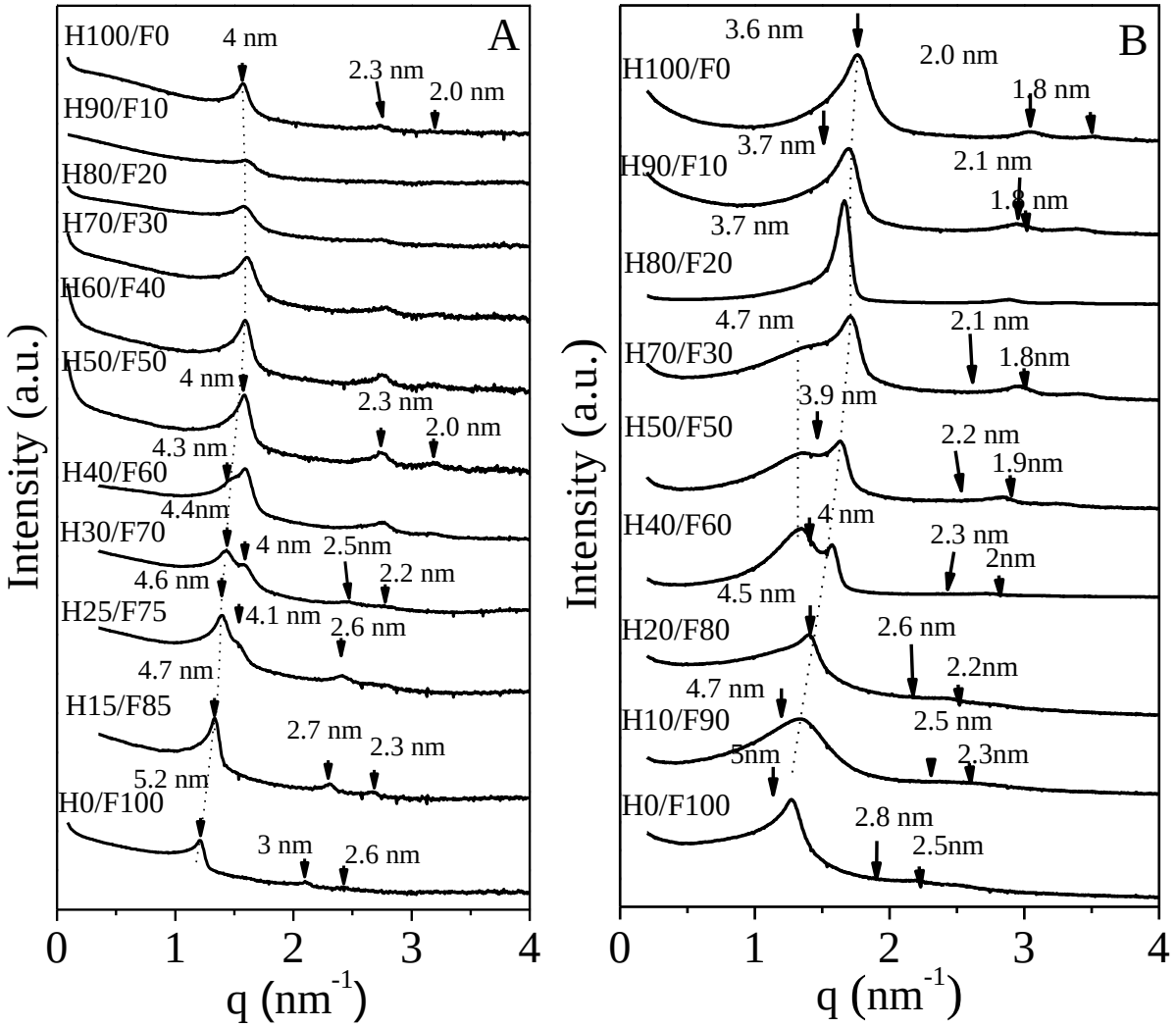
A
H100/F0
4 nm
2.3 nm
2.0 nm
H90/F10
H80/F20
H70/F30
H60/F40
H50/F50
4 nm
2.3 nm
2.0 nm
4.3 nm
H40/F60
4.4nm
H30/F70
4 nm
2.5nm
4.6 nm
2.2 nm
H25/F75
4.1 nm
2.6 nm
4.7 nm
H15/F85
2.7 nm
2.3 nm
5.2 nm
H0/F100
3 nm
2.6 nm
Intensity (a.u.)
0
1
2
3
4
q (nm-1)
B
3.6 nm
2.0 nm
H100/F0
1.8 nm
3.7 nm
H90/F10
2.1 nm
1.8 nm
3.7 nm
H80/F20
4.7 nm
2.1 nm
H70/F30
1.8nm
3.9 nm
H50/F50
2.2 nm
1.9nm
H40/F60
4 nm
2.3 nm
2nm
4.5 nm
H20/F80
2.6 nm
2.2nm
4.7 nm
H10/F90
2.5 nm
5nm
2.3nm
H0/F100
2.8 nm
2.5nm
Intensity (a.u.)
0
1
2
3
4
q (nm-1)

**Figure 5**

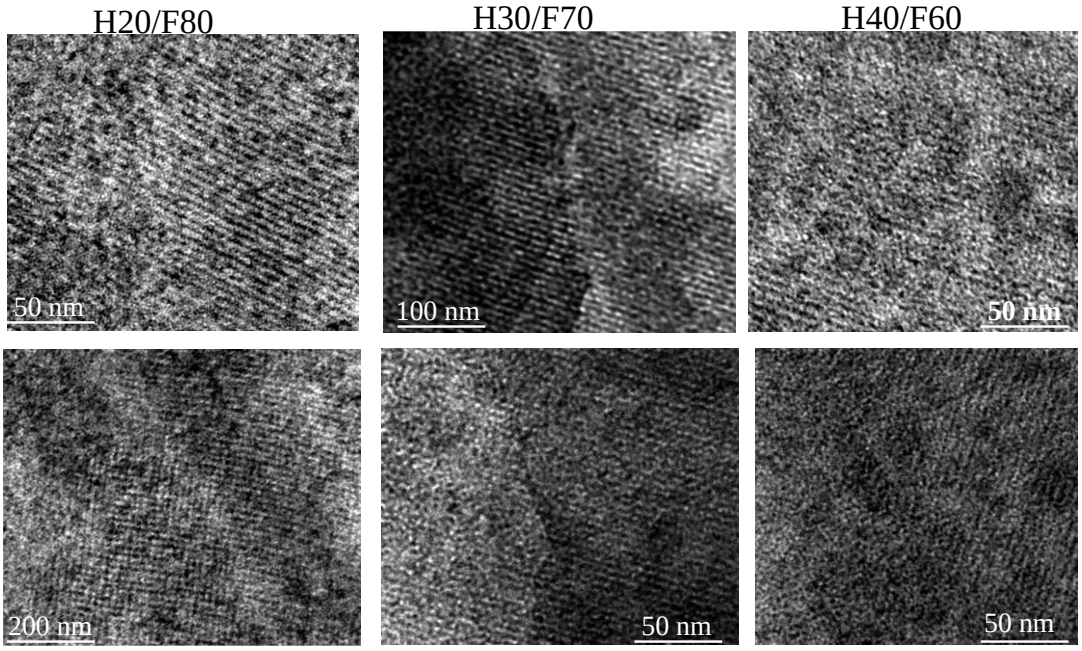

**Figure 6**

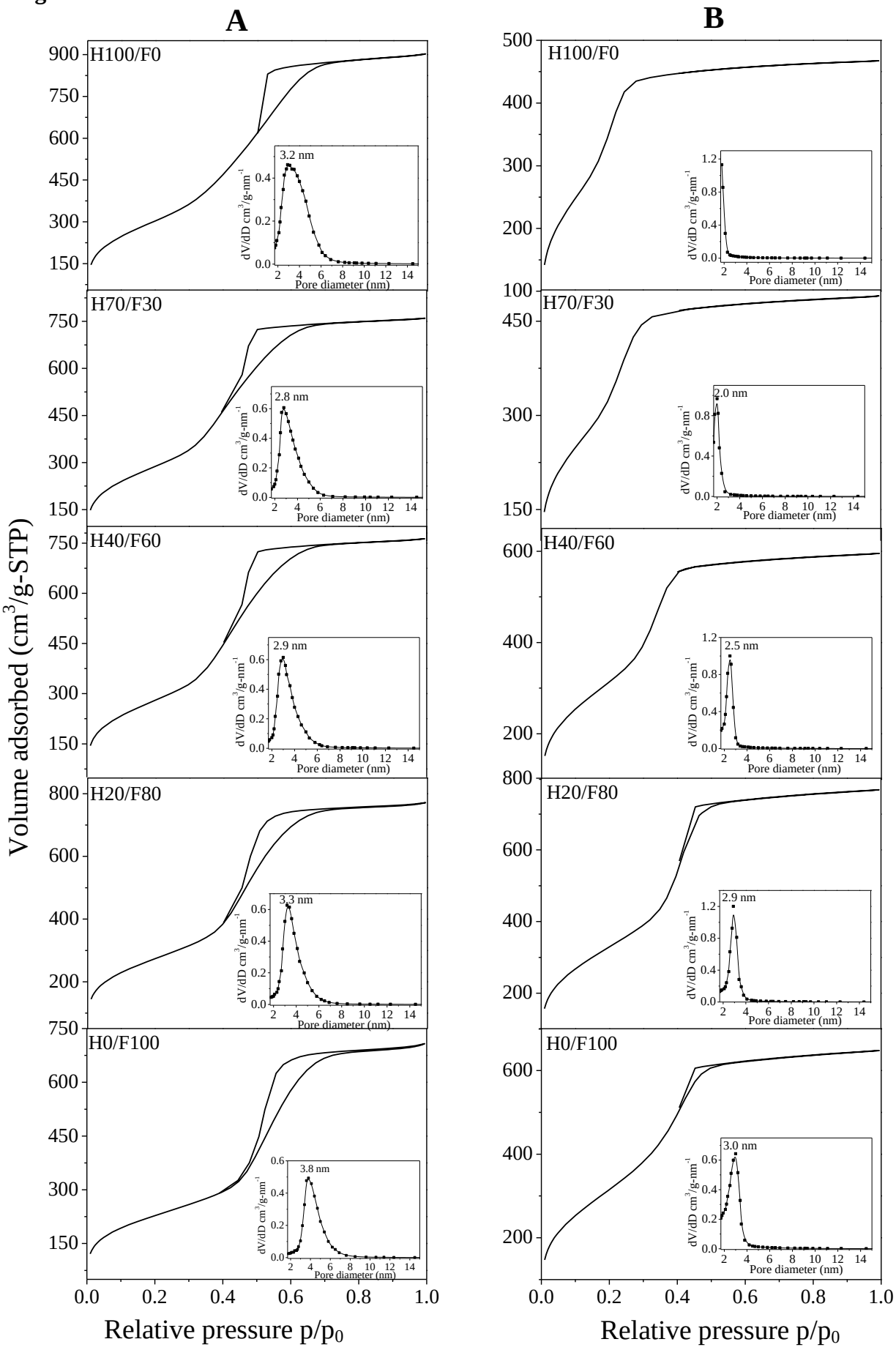
A
B
H100/F0
H70/F30
H40/F60
H20/F80
H0/F100
3.2 nm
2.8 nm
2.9 nm
3.3 nm
3.8 nm
2.0 nm
2.5 nm
2.9 nm
3.0 nm
dV/dD cm3/g-nm-1
Pore diameter (nm)
Volume adsorbed (cm3/g-STP)
Relative pressure p/p0

**Figure7**

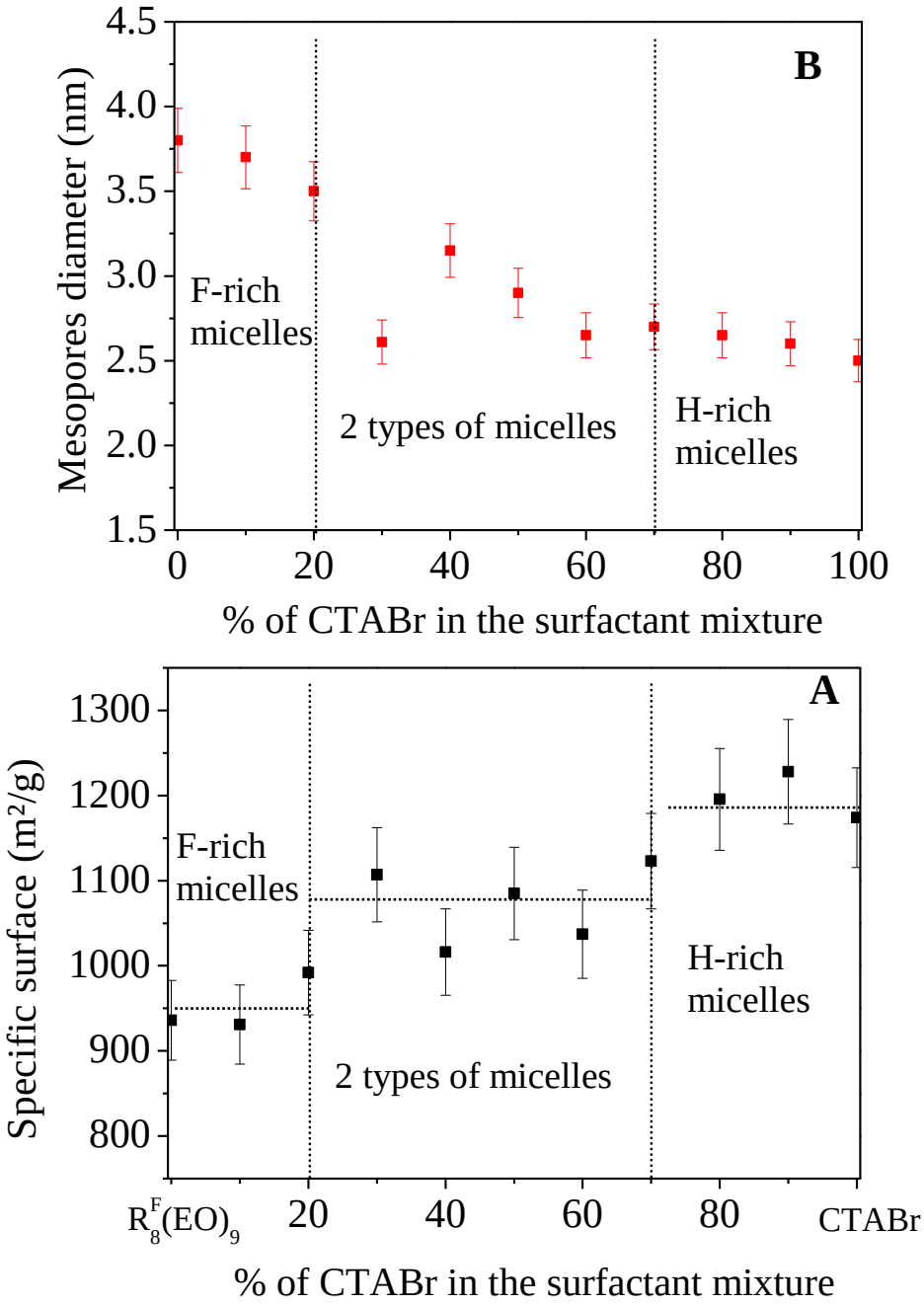
B
Mesopores diameter (nm)
4.5
4.0
3.5
3.0
2.5
2.0
1.5
0
20
40
60
80
100
F-rich micelles
2 types of micelles
H-rich micelles
% of CTABr in the surfactant mixture
A
Specific surface (m²/g)
1300
1200
1100
1000
900
800
F-rich micelles
2 types of micelles
H-rich micelles
R8F(EO)9
20
40
60
80
CTABr
% of CTABr in the surfactant mixture

**Figure 8**